Materials & Design 218 (2022) 110723

Contents lists available at ScienceDirect

Materials & Design

journal homepage: www.elsevier.com/locate/matdes

Nanoscale creep behavior and its size dependency of a Zr-based bulk metallic glass manufactured by selective laser melting

Siqi Liu [a], Zexin Chang [a,b,e], Yuequn Fu [a], Yuyu Liu [a,c], Meichao Lin [a], Xiaobo Ren [d], Wenxian Wang [e], Zhiliang Zhang [a], Jianying He [a,*]

[a] NTNU Nanomechanical Lab, Department of Structural Engineering, Norwegian University of Science and Technology (NTNU), Trondheim 7491, Norway
[b] College of Materials Science and Engineering, Taiyuan University of Science and Technology, Taiyuan 030024, PR China
[c] School of Material Science and Engineering, China University of Mining and Technology, Xuzhou, Jiangsu 221008, PR China
[d] Materials and Nanotechnology, SINTEF Industry, NO-7465 Trondheim, Norway
[e] College of Materials Science and Engineering, Taiyuan University of Technology, 79 West Yingze Street, Taiyuan 030024, PR China

HIGHLIGHTS

- The nanoscale creep behavior of an SLM-ed MG were investigated by nanoindentation.
- The size effect was found to exist in the creep deformation process.
- The creep resistance decreased with the increasing peak loads.
- A potential mechanism for this creep size effect was revealed.

GRAPHICAL ABSTRACT

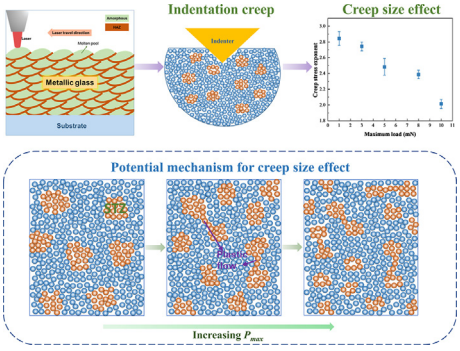

ARTICLE INFO

Article history:
Received 27 December 2021
Revised 23 April 2022
Accepted 3 May 2022
Available online 11 May 2022

Keywords:
Bulk metallic glass
Additive manufacturing
Selective laser melting
Shear transformation zone
Nanoindentation
Creep behavior

ABSTRACT

Nanoscale creep behaviors of metallic glasses (MGs) have gathered considerable interests in recent years, owing to their distinct atomistic mechanisms of plasticity. Additive manufacturing (AM) is a burgeoning technique for manufacturing MGs, the nanoscale creep characteristics and creep mechanism of the AM-ed MGs, however, remain ambiguous. In this work, the nanoscale creep behavior and creep size effect of a selective laser melted (SLM-ed) Zr-based MG were investigated by using nanoindentation. The creep stress exponent (n) and shear transformation zone (STZ) volume, as the indicators of the creep mechanism, were estimated. The n values are in the range of 2–3, and STZ volumes are around 2 nm^3. The creep resistance of the MG was found to decrease with the increasing applied peak loads. A potential mechanism for this creep size effect was revealed: the smaller of the STZ volume, as well as the greater ratio of plastic flow under the higher maximum load, are responsible for the decreasing tendency of creep resistance. This research gives a comprehensive understanding of the atomistic mechanisms in the AM-ed MG during the nanoscale creep deformation process and can serve as a reference for improving the plasticity and further engineering applications.

* Corresponding author.
E-mail address: jianying.he@ntnu.no (J. He).

https://doi.org/10.1016/j.matdes.2022.110723
0264-1275/

1. Introduction

Metallic glasses (MGs), also terms as amorphous alloys, are a species of promising materials with unique disordered atomic structures in the absence of long-range order [1,2]. MGs, unlike crystalline metallic materials, have an unusual microstructure that is devoid of well-defined structural defects such as dislocations and twins that can be detected using a transmission electron microscope [3,4]. The atomistic mechanisms of the plastic deformation behavior in MGs, consequently, are distinct from those in crystalline metals that are dislocation-mediated. In general, most bulk MGs are fabricated by conventional processing methods such as casting, pulsed laser quenching, and melt spinning, etc. [5]. However, these manufacturing methods are limited to dimensions that are less than 30 mm for most bulk MGs [6,7]. Additive manufacturing (AM), an emerging technique, can overcome the drawbacks of the size and geometry limitations of the conventional methods, and thus unlock the potential for the industrial applications of MGs [8].

AM is an innovative technology that builds three-dimensional (3D) parts layer-by-layer guided by a computer-aided-design (CAD) model [9,10]. The superiority of AM lies in the fast fabrication speed and the great shape-design freedom [11-13]. Furthermore, the rapid fabrication and relatively small melting volume in the additive manufactured (AM-ed) metals result in intrinsically high cooling rates (10^6-10^8 K/s) [14,15]. Such high cooling rates, as a consequence, are conducive to obtaining a glassy state from the metallic melt and fabricating the bulk MGs [16]. Selective laser melting (SLM) is one kind of powder bed fusion (PDF) process, and it has been promisingly applied to manufacture bulk MGs or MG coatings in recent years [17]. The SLM process may lead to distinct microstructure and higher defect density in MGs. Therefore, the mechanical properties can be largely influenced by the SLM process, requiring an in-depth investigation.

Due to the viscoelastic characteristic of MGs, creep behavior, as a type of time-dependent plastic property, has attracted significant interest in both academic and industrial viewpoints [18]. It is crucial to gain insight into the underlying mechanism of the creep deformation of MGs, as well as the process-structure-property relationship with regard to the creep behaviors in MGs [19]. The nanoindentation creep test is an appropriate and effective way in comparison with the conventional macroscale creep tests, since it not only provides nanoscale spatial resolution for measuring the deformation behavior, but also requires less time and only a small material volume [20]. During the holding stage of the nanoindentation process, the creep behaviors of the in-situ plastic deformation state of MGs can be captured under the indenter [21]. Different from the conventional creep tests where creep happens at a temperature near the sample's melting point, nanoindentation creep tests can be carried out at room temperature, owing to the high stresses beneath the small indenter involved in indentation creep [22]. In recent years, considerable research efforts have been devoted to investigating the nanoscale creep behavior of various kinds of bulk MGs and MG films fabricated by conventional methods [21,23-27]. However, limited work has focused on the creep behavior of bulk MGs produced by the AM method, and the creep mechanism of the AM-ed MGs remains to be explored.

In the current work, the nanoscale creep behaviors of an SLM-ed Zr-based MG were investigated by nanoindentation technique, with the 500 s holding time. Five different maximum loads were applied for studying the size effect on the creep behaviors. The underlying mechanisms of the creep behaviors and creep size effect were analyzed by the theoretical models.

2. Material and methods

2.1. Material and sample preparation

Amorphous Zr50Ti5Cu27Ni10Al8 (at.%) powders (supplied by Advanced Technology &Materials Co., Ltd.) were used and prepared by high-pressure inert gas atomization. The powder particles had near smooth surfaces with sizes ranging from 5 to 40 μm. A 100 mm × 100 mm × 10 mm pure zirconium plate was used as a substrate. Before SLM, the substrate surface was first ground using a silicon carbide paper to remove surface oxides, and then cleaned with ethanol. The laser additive manufacturing experiments were conducted using a BLT- A160 system. The diameter of the laser beam was 80 μm, and the laser power was 150 W. The laser scanning speed relative to the substrate surface was 1.2 m/s. A 30% overlapping was used between two neighboring tracks. During the laser processing, argon was used as the shielding gas.

The sample was cut from the middle part of the SLM-ed compound with a size of 1 cm × 1 cm × 0.5 cm. Then the sample was polished and etched with the mixture of H_2O, HNO_3, and HF (10:10:1 in volume ratio). The phases in the AM-ed MG were investigated by X-ray diffraction (XRD, TongDa TD-3500) using Cu Kα irradiation with a 2θ range of 20–80°. The thermal property of this MG was investigated by NETZSCH STA 449F3 differential scanning calorimetry (DSC) at a heating rate of 10 K/min. The microstructure was studied by using scanning electron microscopy (SEM). The SEM (FEI, APREO) was operated at 20 kV accelerating voltage, and a solid-state backscattered electron (BSE) detector was used. The chemical composition has been investigated by energy-dispersive X-ray spectroscopy (EDS). The SEM and EDS mapping results were shown in Fig.S2.

2.2. Nanoindentation process

The nanoindentation creep tests were performed on the polished surfaces of the Zr-based MG tip at room temperature, by using Hysitron Tribo-indenter TI 950 equipped with a Berkovich indenter. The tests were conducted on a load-controlled mode, the holding time for extracting creep property was set as 500 s, and each test ran at the constant loading and unloading rate of 0.5 mN/s. In order to study the effect of applied peak loads on the creep behavior, the maximum loads were set at 1 mN, 3 mN, 5 mN, 8 mN, and 10 mN. At least 10 indents were performed at each condition to ensure repeatability, and a 5 μm nanoindentation spacing was applied to refrain from the potential influence of the overlapping plastic zones. In this investigation, the indents were performed only on the fully amorphous structure in the interior of the molten pools, as illustrated in Fig.S1. The heat-affected zone (HAZ) where the crystallization may happen during the reheating process has not been considered. The difference in hardness and reduced modulus in HAZ and amorphous parts are shown in Fig.S3 and Table S1.

3. Classic deformation models in MGs

Several models have been proposed for describing the plasticity of MGs, which are mainly based on two atomic-scale mechanisms, namely free volume theory and shear transformation zones (STZs) [27-29]. The free volume model can describe the mechanical property in a simple style, but it has been challenging to explain the origin of the plastic deformation in MGs [30]. Currently, STZ theory has become the most widely accepted model for associating with the mechanical properties. STZs can be regarded as the local plas-

ticity event or the cluster of atoms in a relatively loosely packed region as the source of plastic flow [31]. As stated by the elastic model, plastic deformation in MGs can be regarded as the flow event [32]. In theory, a flow event in MGs is the process in which a system escapes from one local minimum to another, or the process where the barrier between adjacent local minima disappears under the applied temperature or stress [3]. On the basis of the concept of potential energy landscape (PEL), MGs possess two main flow modes: the slow α-mode which is an irreversible hopping event; and the relatively fast β-mode (or Johari-Goldstein) relaxations which are reversible [3,33]. In order to associate the STZ with the physical properties, the cooperative shear model (CSM), which is proposed by Johnson and Samwer, merged the concept of STZs into the PEL perspective for interpreting the deformation mechanisms and rheological properties in MGs [34]. As illustrated in Fig. 1, during plastic deformation, the STZ events are restricted inside the peripheral matrix and correlate to reversible β-mode relaxation. When the applied temperature (T) or stress (τ) reaches a critical threshold, the peripheral elastic matrix collapses, leading to large-scale atomic migration and the plastic flow which corresponds to the irreversible α-relaxation [3,33,35].

4. Results and discussions

4.1. XRD and DSC results

The XRD pattern of the AM-ed Zr-based MG is shown in Fig. 2a. The XRD pattern of the AM-ed MG displays the broad diffraction maxima ($2\theta \sim 38°$) which indicates the material mainly contains the amorphous phase. In addition, two weak crystalline peaks ($2\theta \sim 36°$ and $\sim 39°$) can be also observed which demonstrates a small amount of crystalline phase inside the HAZ. As shown in the DSC trace in Fig. 2b, the glass transition temperature (T_g) of this sample is measured as 683 K and the onset temperature of the crystallization (T_x) is 763 K.

4.2. Representative P-h curves

The representative load versus displacement (P-h) curves under different maximum loads are displayed in Fig. 3a. These curves contain the loading, holding, and unloading stages, in which the creep behavior happens in the holding stage. As can be seen in Fig. 3a, the total displacement, as well as the creep displacement in the holding stage, increase with the applied maximum load. Furthermore, a series of displacement bursts, termed as "pop-in" events or serration, can be observed in the loading stage of the curves. These serrations are associated with the initiation and expansion of the shear bands underneath the indenter tip and have been observed in other types of MGs [36-38]. The hardness and reduced modulus, the two most common nanomechanical properties acquired by nanoindentation, are calculated by the recognized Oliver and Pharr (O-P) methods [39,40] and presented in Fig. 3b. It can be seen that the values of hardness and reduced modulus decrease with the increasing maximum load, which indicates the distinct indentation size effect (ISE) in this MG. The size dependence of mechanical behavior is generally related to the inherent length scale. In crystalline materials, ISE is commonly rationalized by the strain gradient plasticity theory which was developed by Nix and Gao [41]. Differing from the crystalline materials, MG has no geometrically necessary dislocations (GNDs), and thus the ISE in MGs cannot be explained by strain gradient plasticity theory. According to the previous reports, the activities of STZs controlled by indentation size or deformation volume account for the ISE in MGs [42]. When the indentation depth is shallow, the highly

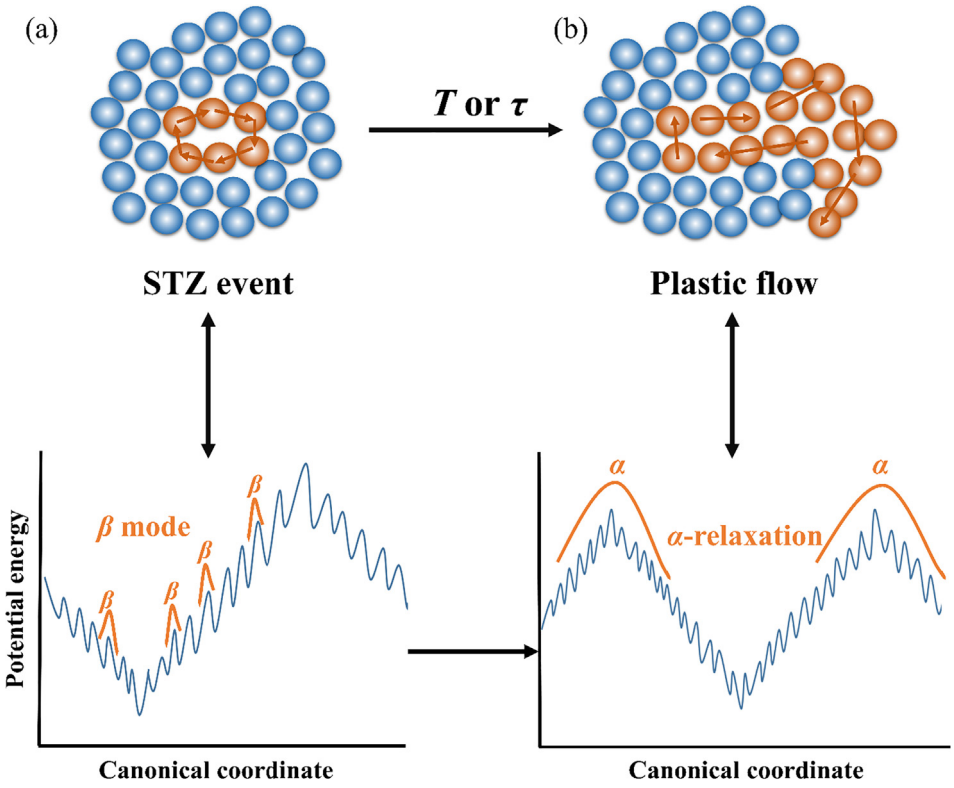

Fig. 1. The two-dimensional schematic diagram of (a) STZ activation event corresponds to β-mode relaxation, and (b) plastic flow corresponds to the α-mode relaxation [3]. The blue balls represent atoms in the elastic matrix, and the orange balls represent the high mobility atoms. (For interpretation of the references to colour in this figure legend, the reader is referred to the web version of this article.)

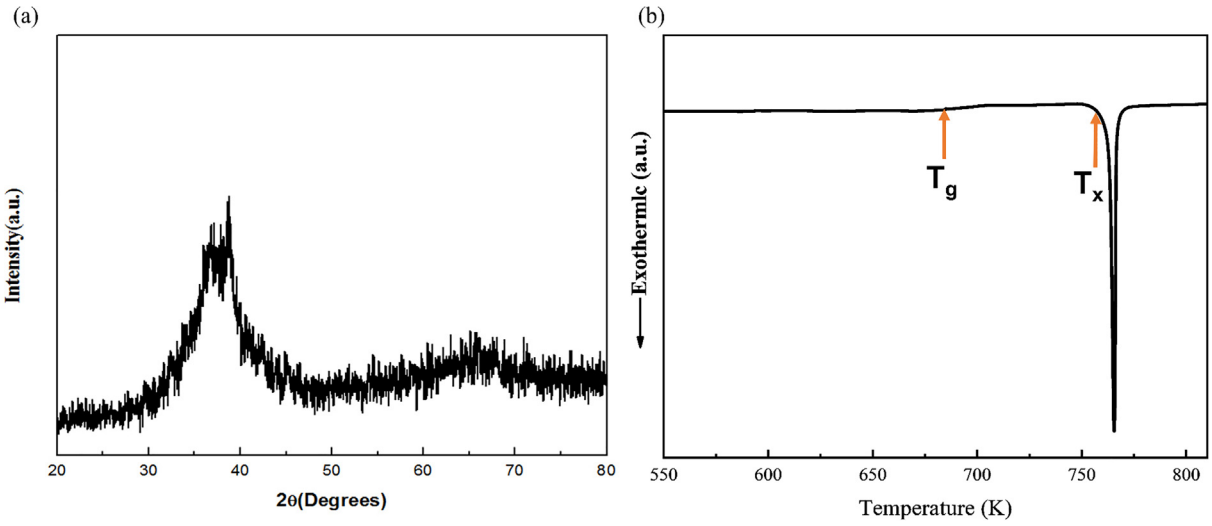

Fig. 2. (a) Typical XRD pattern of the AM-ed Zr-based MG. (b) DSC trace of the sample, showing $T_g \approx 683$ K and $T_x \approx 763$ K.

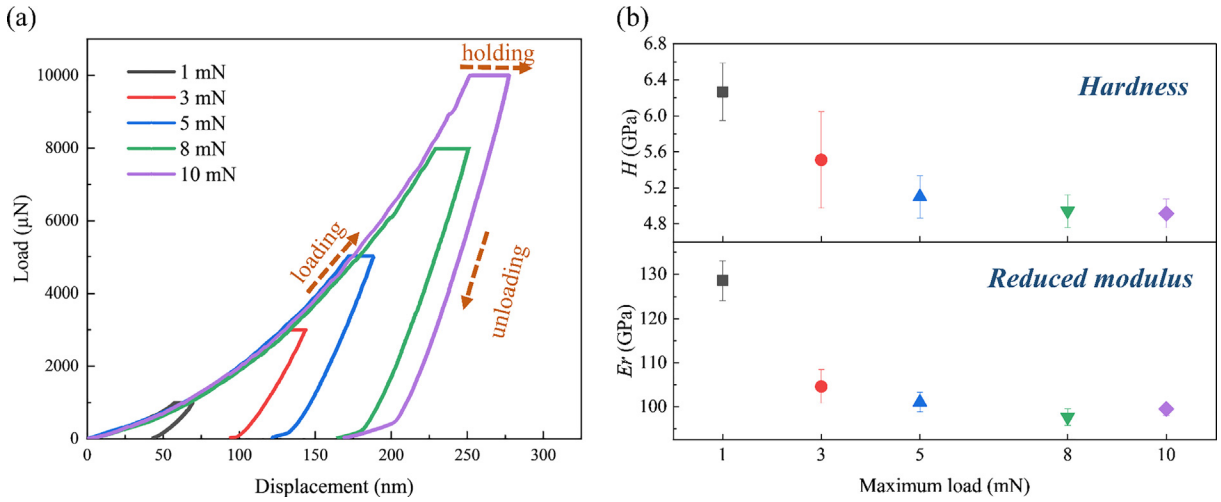

Fig. 3. (a) The representative Load-Displacement (*P-h*) curves under different maximum loads; (b) variation of hardness and reduced modulus with the varying maximum load.

stressed volume under the indenter is limited for the activation of STZs and the subsequent shear bands. As the depth of penetration increases, the deformation volume increases, and thus a lower hardness may be observed due to the higher activities of STZs and shear bands [42]. Furthermore, the excessive free volume can lead to the decrease of the atomic bonding [43]. Therefore, the reduction of the reduced modulus with the applied load can be attributed to the comprehensive effect of the higher activities of STZs and the decrease of atomic bonding.

4.3. Nanoscale creep deformation

Fig. 4a presents the representative creep displacement versus holding time curves under different maximum loads, showing the total creep displacements increase with the applied maximum loads. Given the viscoelastic nature of MGs, models in which several basic spring and dashpot units are connected in series or parallel can describe the creep deformation behavior of MGs [44]. In general, the spring units obeying Hooke's law represent the elastic matrix, and the dashpot units following Newton's law represent the viscoplastic component [44]. Therefore, in an effort to further analyze the creep behavior of MG in detail, the generalized Kelvin model, which is most commonly used for MGs, is applied to fit the creep curves. As demonstrated in Fig. 4b, the generalized Kelvin model connects *n* Kelvin units (2 units for simplification) and a Maxwell unit in series, and thereinto the Kelvin unit consists of a linear elastic spring and a linear viscous dashpot in parallel [19,45]. Therefore, the creep displacement contains the strain of Kelvin units (ε_{K1}, ε_{K2}) and the strain of Maxwell unit (ε_{Ms}, ε_{Md}), and can be described by the following equation [19,46]:

$$h = h_e + h_1\left(1 - e^{-t/\tau_1}\right) + h_2\left(1 - e^{-t/\tau_2}\right) + t/\mu_0 \quad (1)$$

where h_e represents the indentation displacement at the first spring, h_1 and h_2 are the indentation depth at the two Kelvin elements, τ_1 and τ_2 represent the retardation time for the Kelvin elements, t is the holding time and μ_0 is the constant related to the viscosity coefficient of the Maxwell dashpot. These fitting parameters for all curves are summarized in Table 1.

Fig. 4c shows a typical depth versus holding time curve under 8 mN and the well-fitted curve by using Eq. (1), and the curves under other peak loads are presented in Fig.S4 The creep displacement curves can be split into two stages: the primary creep stage corre-

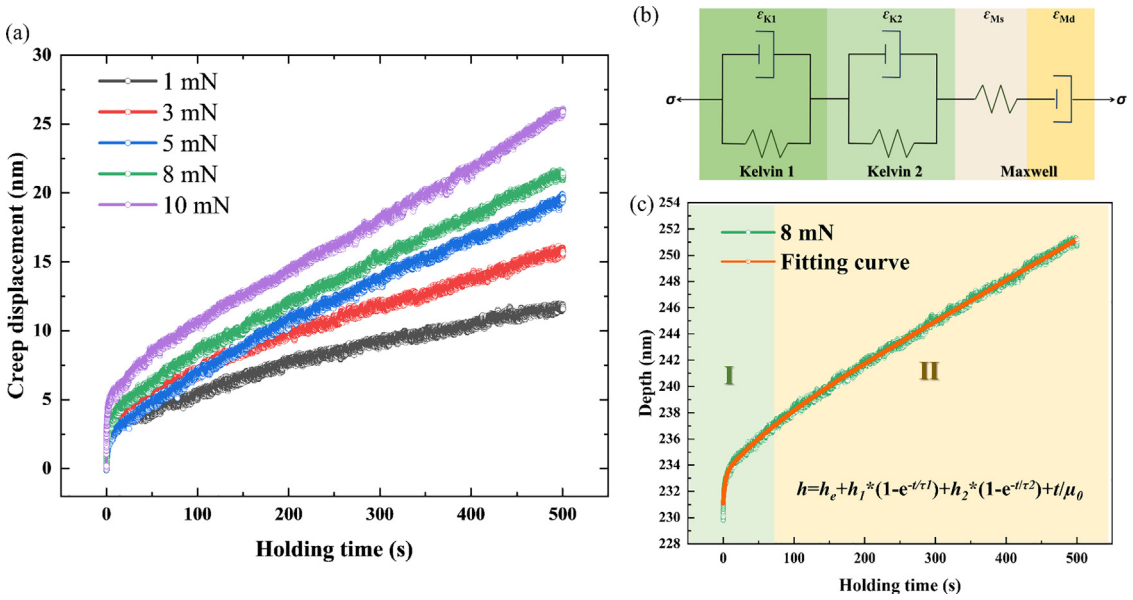

Fig. 4. (a) The creep displacement versus holding time curves under different maximum loads. (b) The schematic diagram of the generalized Kelvin model used for analyzing creep curves, including a Maxwell unit and two Kelvin units. (c) The representative fitting curve under a maximum load of 8 mN by applying the generalized Kelvin model, containing two stages: primary stage (I) and steady-state stage (II).

Table 1
The fitting parameters of creep curves under different maximum loads based on the generalized Kelvin model.

P_{max}	h_e (nm)	h_1 (nm)	h_2 (nm)	τ_1 (s)	τ_2 (s)	μ_0 (S/Nm)	R^2
1 mN	58.71	1.658	4.619	2.664	182.7	104.8	0.9960
3 mN	128.4	2.417	3.202	1.889	78.42	52.16	0.9974
5 mN	171.9	1.856	5.038	1.998	173.3	40.38	0.9990
8 mN	231.1	2.16	2.392	2.944	72.45	32.14	0.9990
10 mN	252.9	2.976	2.436	0.66	25.97	26.56	0.9989

sponds to the process of rapidly increasing, where these two Kelvin units play a dominant role; and the steady-state stage represents the velocity of increase of the creep displacement that tends to be stable, in which Maxwell dashpot plays a leading role [19]. Therefore, the boundary between the two stages can be defined by the value of τ_2.

In order to better understand the creep behaviors in MGs, the generalized Kelvin model can also be used to deduce other time-dependent properties. Creep compliance, $J(t)$, defined as the strain variations under instantaneous application of constant stress, is an essential property that represents the rheological behavior of viscoelastic materials with respect to time [47,48]. It can be obtained from the generalized Kelvin model as the following [19,46,49]:

$$J(t) = \frac{A_0}{P_0 h_{in}} h(t) = \frac{A_0}{P_0 h_{in}} [h_e + h_1 \left(1 - e^{-\frac{t}{\tau_1}}\right) + h_2 \left(1 - e^{-\frac{t}{\tau_2}}\right) + \frac{t}{\mu_0}] \quad (2)$$

where A_0 is the contact area at the maximum load, P_0 is the applied maximum load, and h_{in} is the displacement at the end of the loading.

The creep compliance can be determined by Eq. (2) with the fitted parameters in Table 1. The dependency of creep compliance on holding time under five applied maximum loads, as shown in Fig. 5a, shows a similar tendency, i.e., creep compliances are initially nearly constant and subsequently appear to grow progressively with the holding time. The increasing trend of creep compliance has been observed in other types of amorphous alloys and polymers, and it is largely attributed to the softening dispersion or structural relaxation in MGs [48-50]. By comparing the creep compliances under the five maximum loads, it can be found that the values of compliance increase with the increasing applied maximum loads from 1 mN to 8 mN, and then the compliance under 10 mN has a slight decrease, which indicates that the structure of the MG becomes relaxed with the increase of the applied load. In MGs, the creep compliance is reported to be inversely related to the modulus ($J \sim 1/E$) [49], therefore, the increase in compliance reflects the decrease in modulus. It is found that the change tendency of the creep compliance coincides with the change tendency of reduced modulus on the contrary, as shown in Fig. 3b.

Furthermore, the creep retardation spectra, $L(\tau)$, which is the plot of creep compliance versus $\ln(\tau_i)$, represents the distribution functions for the creep compliance [45,51]. The creep retardation spectra are used for a deep comprehension of the viscoelastic behavior as well as the time scale where the viscous process happens [45]. It can also shed light on the dynamic nature of the MGs and describe the defect activation in detail during the creep process [19,44]. $L(\tau)$ can be derived from the inverse Laplace transform of the creep compliance function as the following equation [52]:

$$L(\tau) = \left[\left(1 + \frac{t}{\tau_1}\right)\frac{h_1}{\tau_1} e^{-\frac{t}{\tau_1}} + \left(1 + \frac{t}{\tau_2}\right)\frac{h_2}{\tau_2} e^{-\frac{t}{\tau_2}}\right] \frac{A_0}{P_0 h_{in}} t|_{t=2\tau} \quad (3)$$

Fig. 5b displays the creep retardation spectra of the AM-ed MG under different maximum loads. There are two separate retardation peaks for all of the relaxation spectra, which demonstrates that two different relaxation states exist in the nanoindentation creep process of the MG. Previous studies have proposed that the

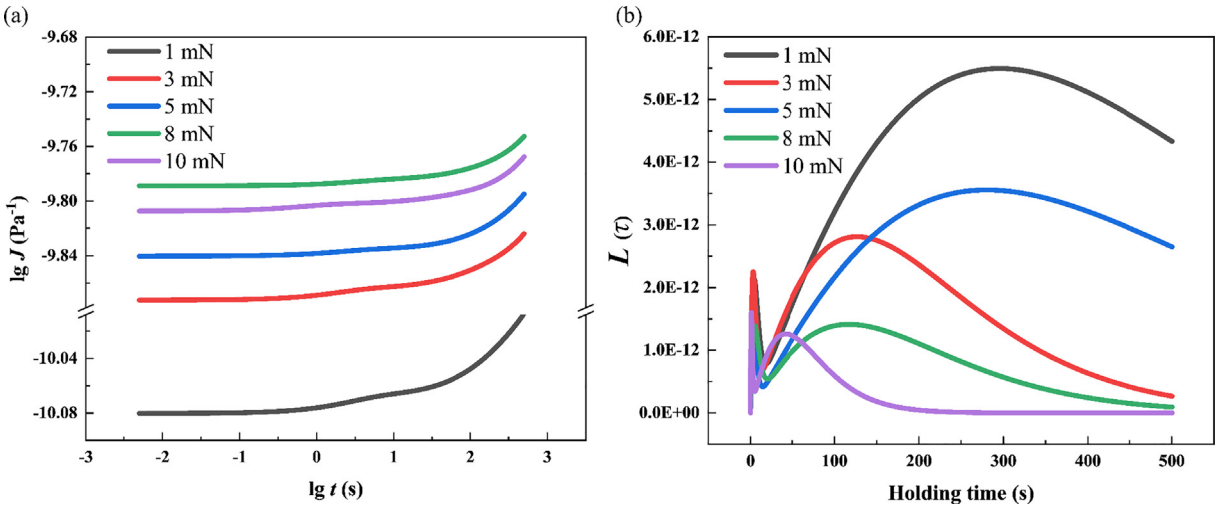

Fig. 5. (a) Creep compliance spectra and (b) Retardation spectra of the SLM-ed Zr-based MG under the different maximum loads.

width and intensity of the peaks are relevant to the size and state of the defects in MG, and each peak represents the distinct material-transport mechanisms or different flow defects [36,53]. It can be seen that the first peaks are narrow and sharp, representing the fast relaxation (β-mode relaxation), while the secondary peaks that signify the slow relaxation (α-relaxation) are relatively broad. As shown in Fig. 5b, the intensity of the relaxation peaks under 1 mN are the largest, and the peaks under 10 mN have the lowest intensity, which indicates that the structure of MG is more relaxed under the lower maximum load. The first peaks, in which the characteristic relaxation times are nearly independent of the maximum loads. Differently, the relaxation times of the second peaks are more sensitive to the maximum loads, and the characteristic relaxation time becomes shorter with the increasing maximum loads except 5 mN. This result implies that the increasing applied maximum loads exhibit an apparent positive effect on the activation of the α-relaxation process in SLM-ed MG.

4.4. Room-temperature creep mechanism at the nanoscale

Creep stress exponent (n) or creep strain rate sensitivity (m) is an important indicator for the creep mechanism in both crystalline materials and amorphous alloys. It should be noted that n and m have a reciprocal relationship ($n = 1/m$), and n as the indicator is applied in the current work. For the crystalline alloys, the creep mechanism can be diffusion-dominant (n = 1–2) or dislocation-dominant (n = 3–8) [25]. In MGs, the correlation between n and creep mechanism is still indefinite at present. However, it has been proposed that if $n \sim 1$, the flow is Newtonian viscous, meaning the viscosity is independent of strain rate; if $n > 1$, the flow is inhomogeneous non-Newtonian, meaning the forced flow is achieved by sudden and localized atomic or molecular rearrangement. [3,54,55]. The relatively higher n value implies the higher creep resistance and the lower flow mobility in MGs [33]. Creep stress exponent (n) can be evaluated from the steady-state creep stage by the following expression:

$$n = \frac{\partial ln\dot{\varepsilon}}{\partial ln\sigma} \tag{4}$$

where $\dot{\varepsilon}$ represents the strain rate, and σ refers to the effective stress. Here, the strain rate ($\dot{\varepsilon}$) for indentation creep tests can be estimated by the following equation proposed by Mayo and Nix [56]:

$$\dot{\varepsilon} = \frac{1}{h_i}\frac{dh}{dt} \tag{5}$$

where h_i refers to the instantaneous indenter displacement, dh/dt is the creep rate that is fitted and differentiated by the empirical formula [57], $h_i = h_0 + at^b + ct$, where h_0 is the displacement at the starting of creep, t is the creep time in the holding stage, and a, b, and c are fitting constants. The effective stress (σ) can be calculated from instantaneous hardness H_i ($\sigma = H_i/C$), where C is a constraint factor and usually ~3 for metallic materials [58]. H_i is taken as the applied load (P) divided by the projected contact area (A), and could be obtained by $P/(24.5h_i^{\ 2})$ for the Berkovich indenter [13].

The creep stress versus holding time curves under the various maximum loads are plotted in Fig. 6a. It can be seen that all of the curves display the reduced tendency of stress during the holding time, and the creep stress decreases with the applied maximum loads. Fig. 6b presents the creep strain rate curves as a function of the holding time. During the holding time, the creep strain rates decrease rapidly at the transient creep stage, and subsequently come to nearly the constant value in the order of 10^{-4} at the steady-state stage. In crystalline materials, the diminishing creep strain rates are attributed to the dynamic equilibrium between dislocation generation ($\dot{\rho}^+$) and annihilation ($\dot{\rho}^-$) in the creep steady stage [13,59]. In a similar manner, the creep strain rate in the steady-state stage, for MGs, can be considered as a dynamic equilibrium between the free volume formation that results in plastic flow softening, and the annihilation that contributes to the hardening [24,25]. Furthermore, as shown in the inset of Fig. 6b, the creep strain rate decreases relatively slower under the smaller maximum load, in other words, a higher applied maximum load results in the decreased transition time from the transient stage to the steady-state stage.

Fig. 6c displays the curves of lnσ-ln $\dot{\varepsilon}$, which demonstrates the deduction of the creep stress exponent. As can be seen, the slope of the curves decreases with the decreasing creep stress, and then comes to a constant in the steady-state stage. The creep stress exponent, consequently, can be estimated by the slope in the steady-state stage. The obtained values of n under the various maximum loads are plotted in Fig. 6d and summarized in Table 2. The values of n are in the range of 2–3, which means the flow in the MG is non-Newtonian [54]. Furthermore, when compared to other Zr-based MG generated by traditional techniques in the literature [25,27,36,60], the n values in our study are relatively small, sug-

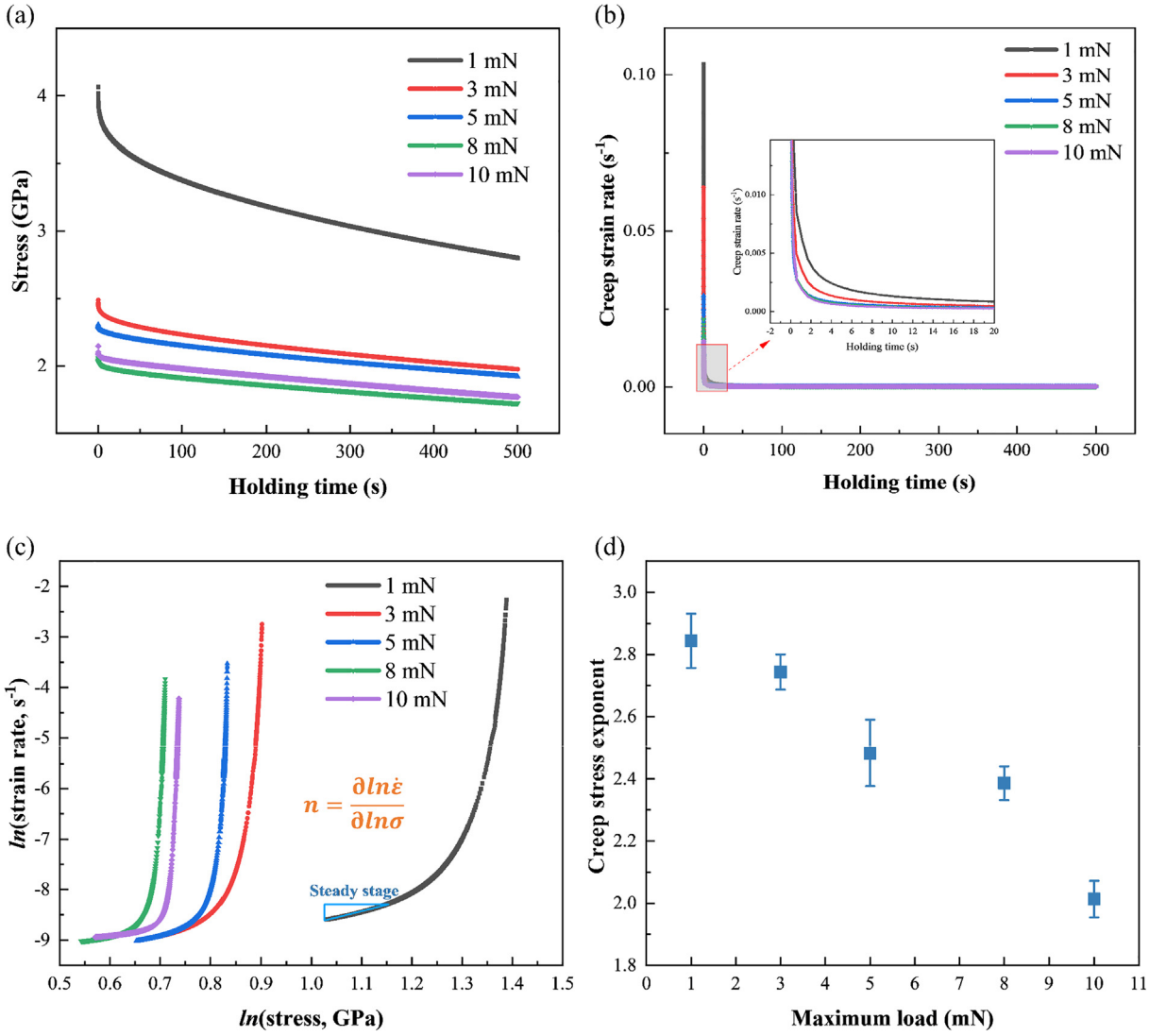

Fig. 6. (a) Creep stress versus holding time; (b) creep strain rate curves as a function of holding time, the inset shows the amplification for displaying the details; (c) ln(strain rate) versus ln(stress) curves showing the calculation of creep stress exponent; (d) the values of creep stress exponent under the different maximum loads.

Table 2
Summary of creep stress exponent, STZ volume, and activation volume under the various maximum loads.

P_{max}	1 mN	3 mN	5 mN	8 mN	10 mN
Creep stress exponent, n	2.843 ± 0.087	2.743 ± 0.056	2.483 ± 0.106	2.387 ± 0.055	2.013 ± 0.058
STZ volume (nm^3)	1.975 ± 0.076	2.181 ± 0.241	2.119 ± 0.071	2.099 ± 0.118	1.781 ± 0.046
Activation volume (nm^3)	0.089 ± 0.003	0.098 ± 0.010	0.095 ± 0.003	0.094 ± 0.005	0.080 ± 0.002

gesting that the AM process leads to different defect densities that impact the creep resistance. It can be found that the creep stress exponent of the AM-ed MG also exhibits apparent size dependence, that is, the n values decrease with the raising of the applied maximum load, which suggests the creep resistance decrease. This is contrary to the other metallic alloys including both crystalline alloys and metallic glasses reported in previous literature [22,26,61,62], implying a new mechanism behind the result in the SLM-ed MG that requires further exploration.

On account of the thermally activated process nature of creep, the activation volume, V^*, is another important parameter to understand the creep behavior. The activation volume can be evaluated by the following equation [63]:

$$V^* = MkT\left(\frac{\partial ln\dot{\varepsilon}}{\partial\sigma}\right) = \frac{\sqrt{3}nkT}{\sigma} \quad (6)$$

where M is the Taylor factor estimated with von Mises relation ($M = \sqrt{3}$), k is Boltzmann's constant, and T is the temperature in Kelvin.

In fact, the STZs can be regarded as the plastic unit in MGs, and the activation volume is simply associated with elementary shear to the STZ volume [64]. STZ volume and activation volume under small-scale deformation can be characterized by indentation creep deformation, statistical analysis of first pop-in data in nanoindentation, on-chip tensile testing, etc. [65-67].

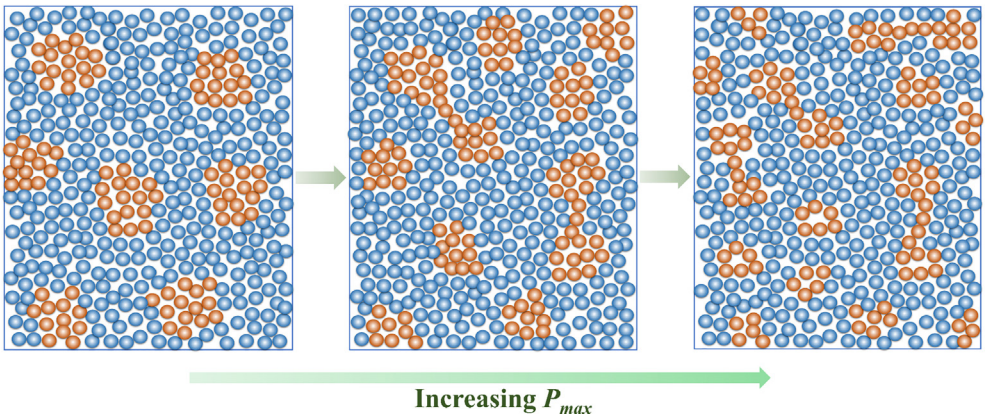

Fig. 7. The schematic illustration of the potential mechanism of the size effect on creep behavior. The STZ volume decreases with the increasing applied maximum load (P_{max}), meanwhile, the plastic flow (percolation of the STZs) is more likely to occur at a higher P_{max}. The blue balls represent atoms in the elastic matrix, the orange balls represent the high mobility atoms in the STZs, respectively. (For interpretation of the references to colour in this figure legend, the reader is referred to the web version of this article.)

It has been widely accepted that the plastic deformation, as well as the creep properties, are closely related to the activation of STZs in MGs [18,68]. In general, lower activation energy (or energy barrier) is required for smaller STZs, giving rise to more amount of STZ events to be activated during the creep deformation process [69]. On the basis of the cooperative shear model (CSM) proposed by Johnson and Samwer [34], the activation energy of STZ is defined as:

$$W_{STZ} = 4RG\gamma_C{}^2\left(1-\frac{\tau}{\tau_C}\right)^{3/2}\xi\Omega \tag{7}$$

where R and ξ are the constants, G is the shear modulus, γ_C is the average elastic limit, τ and τ_C are the shear yield stresses at the temperature in Kelvin and 0 K, respectively, and Ω represents the STZ volume.

Consequently, the STZ volume (Ω) can be deducted by direct differentiation of the activation energy (W_{STZ}):

$$\Omega = \frac{\tau_C}{6RG\gamma_C{}^2\left(1-\frac{\tau}{\tau_C}\right)^{1/2}\xi}V^* \tag{8}$$

By taking Eq.(6) to Eq.(8), the STZ volume (Ω) can be rewritten and expressed as follows:

$$\Omega = \frac{nkT}{C'H} \tag{9}$$

where T is the temperature in Kelvin. C' is a constant that equals to $\frac{2R\xi}{\sqrt{3}}\cdot\frac{G\gamma_C{}^2}{\tau_C}\left(1-\frac{\tau_{CT}}{\tau_C}\right)^{1/2}$, in which the constants $R \approx 1/4$, $\xi \approx 3$, $G/\tau_C \approx 9.25$, γ_C = 0.108–0.05 T/T_g, and $\frac{\tau_{CT}}{\tau_C}$ = 1–0.463 T/T_g [70], where T_g is the glass transition temperature, and T_g = 683 K for this MG.

The values of STZ volume and activation volume under the varying peak loads are summarized in Table 2. With the increase of peak load, the STZ volume and activation volume decrease gradually except for the condition under 1 mN. Even though the activation volume and STZ volume under 1 mN is slightly smaller than the condition of 3 mN, the n value that represents the creep resistance under 1 mN is higher. It is noteworthy that the case with a maximum load of 1 mN, which is within the shallow depth regime, is expected to be a different mechanism from others. In this case, the free volume evolution and the interfacial diffusion are the dominant mechanisms [69]. The potential deformation mechanism behind the tendency from 3 mN to 10 mN can be described by the schematic illustration in Fig. 7. As the applied peak load increases, the STZ volume reduces gradually, implying the energy barrier of the STZ activation decreases. Therefore, the STZs are more easily activated, which is responsible for the diminution of creep resistance becomes. As reported in the prior work [68], the basic process of STZ activation is equivalent to the mechanically activated β-mode relaxation. In addition, when the applied load exceeds a critical threshold and the potential energy builds up to a certain amount, the plastic flow that corresponds to the irreversible α-relaxation will be triggered. Therefore, the plastic flow represents α-relaxation needs to be taken into account for the underlying mechanism of the creep size effect. As illustrated in Fig. 7, the plastic flow becomes more likely to happen under a higher maximum load, which is also attributable to the tendency of creep resistance. As a consequence, the decreasing tendency of the creep resistance is largely attributed to the diminution of the STZ volume as well as the greater ratio of plastic flow under the higher maximum load. Furthermore, the values of STZ volume in the current work are around 2 nm^3, which are smaller than the Zr-based MGs manufactured by other methods [36,71,72]. The smaller volume of STZ is responsible for the smaller creep stress exponent and the corresponding creep resistance in the AM-ed MG.

5. Conclusions

The nanoindentation creep behaviors of a selective laser melted (SLM-ed) $Zr_{50}Ti_5Cu_{27}Ni_{10}Al_8$ metallic glass (MG) were investigated at ambient temperature, and the size effect on the creep behavior was explored by applying various maximum loads. The nanoindentation creep curves were analyzed and fitted by the generalized Kelvin model, and the creep compliance, as well as creep retardation spectra, were consequently obtained. The creep mechanism was analyzed by the creep stress exponent (n) and STZ volume on the basis of the cooperative shear model (CSM). The main conclusions can be summarized as follows:

1. The size effect is found to exist in the nanoscale creep deformation process.
2. Two separate retardation peaks are shown in the relaxation spectrums, implying two different types of relaxation states exist in the creep process. The increscent applied maximum loads play a positive role in the activation of the α-relaxation.
3. The values of n are in the range of 2–3, indicating the deformation flow in the SLM-ed MG is non-Newtonian.
4. The n values that represent the creep resistance also exhibit apparent size dependence, i.e., the n values decrease with the applied peak loads. The STZ volumes are around 2 nm^3, and

the activation volumes are near 0.1 nm^3. With the increase of peak load, the STZ volume and activation volume decrease gradually except for the condition under 1 mN.

5. A potential mechanism was revealed based on CSM. With the increasing applied peak loads, the STZ volume and the energy barrier of the STZ activation reduced gradually, meanwhile, the plastic flow became more likely to happen. Therefore, the creep resistance had a decreasing tendency.

CRediT authorship contribution statement

Siqi Liu: Conceptualization, Methodology, Investigation, Writing – original draft, Writing – review & editing, Formal analysis, Visualization, Validation. **Zexin Chang:** Resources, Investigation, Writing – review & editing. **Yuequn Fu:** Writing – review & editing, Formal analysis. **Yuyu Liu:** Investigation, Formal analysis. **Meichao Lin:** Formal analysis. **Xiaobo Ren:** Writing – review & editing. **Wenxian Wang:** Resources, Writing – review & editing. **Zhiliang Zhang:** Writing – review & editing, Supervision. **Jianying He:** Validation, Writing – review & editing, Supervision, Funding acquisition.

Declaration of Competing Interest

The authors declare that they have no known competing financial interests or personal relationships that could have appeared to influence the work reported in this paper.

Acknowledgments

The Research Council of Norway (Grant No. 251068) and the Chinese Scholarship Council are acknowledged for the support of this work. The Research Council of Norway is acknowledged for the support to the Norwegian Micro- and Nano-Fabrication Facility, NorFab, project number 295864.

Appendix A. Supplementary data

Supplementary data to this article can be found online at https://doi.org/10.1016/j.matdes.2022.110723.

References

[1] A. Inoue, Stabilization of metallic supercooled liquid and bulk amorphous alloys, Acta Mater. 48 (1) (2000) 279–306, https://doi.org/10.1016/S1359-6454(99)00300-6.
[2] M. Zhang, Y. Chen, W. Li, On the origin of softening in the plastic deformation of metallic glasses, Int. J. Plast. 116 (2019) 24–38, https://doi.org/10.1016/j.ijplas.2018.12.004.
[3] W.H. Wang, Y. Yang, T.G. Nieh, C.T. Liu, On the source of plastic flow in metallic glasses: Concepts and models, Intermetallics. 67 (2015) 81–86, https://doi.org/10.1016/j.intermet.2015.08.004.
[4] A.L. Greer, Y.Q. Cheng, E. Ma, Shear bands in metallic glasses, Mater. Sci. Eng. R Reports 74 (4) (2013) 71–132, https://doi.org/10.1016/j.mser.2013.04.001.
[5] M.M. Khan, A. Nemati, Z.U. Rahman, U.H. Shah, H. Asgar, W. Haider, Recent Advancements in Bulk Metallic Glasses and Their Applications: A Review, Crit. Rev. Solid State Mater. Sci. 43 (3) (2018) 233–268, https://doi.org/10.1080/10408436.2017.1358149.
[6] A. Inoue, A. Takeuchi, Recent development and application products of bulk glassy alloys, Acta Mater. 59 (6) (2011) 2243–2267, https://doi.org/10.1016/j.actamat.2010.11.027.
[7] H. Liu, Q.i. Jiang, J. Huo, Y. Zhang, W. Yang, X. Li, Crystallization in additive manufacturing of metallic glasses: A review, Addit. Manuf. 36 (2020) 101568, https://doi.org/10.1016/j.addma.2020.101568.
[8] X.P. Li, M.P. Roberts, S. O'Keeffe, T.B. Sercombe, Selective laser melting of Zr-based bulk metallic glasses: Processing, microstructure and mechanical properties, Mater. Des. 112 (2016) 217–226, https://doi.org/10.1016/j.matdes.2016.09.071.
[9] T. DebRoy, H.L. Wei, J.S. Zuback, T. Mukherjee, J.W. Elmer, J.O. Milewski, A.M. Beese, A. Wilson-Heid, A. De, W. Zhang, Additive manufacturing of metallic components – Process, structure and properties, Prog. Mater. Sci. 92 (2018) 112–224, https://doi.org/10.1016/j.pmatsci.2017.10.001.
[10] S. Liu, M. Lin, X.u. Wang, Y. Fu, X. Ren, Z. Zhang, J. He, A framework for predicting the local stress-strain behaviors of additively manufactured multiphase alloys in the sequential layers, Mater. Sci. Eng. A. 832 (2022) 142367, https://doi.org/10.1016/j.msea.2021.142367.
[11] T.D. Ngo, A. Kashani, G. Imbalzano, K.T.Q. Nguyen, D. Hui, Additive manufacturing (3D printing): A review of materials, methods, applications and challenges, Compos. Part B Eng. 143 (2018) 172–196, https://doi.org/10.1016/j.compositesb.2018.02.012.
[12] M. Zenou, L. Grainger, in: Additive manufacturing of metallic materials, Elsevier Inc., 2018, pp. 53–103, https://doi.org/10.1016/B978-0-12-812155-9.00003-7.
[13] S. Liu, D.i. Wan, S. Guan, Y. Fu, X. Ren, Z. Zhang, J. He, Microstructure and nanomechanical behavior of an additively manufactured (CrCoNiFe)94Ti2Al4 high-entropy alloy, Mater. Sci. Eng. A. 823 (2021) 141737.
[14] J. Wegner, M. Frey, M. Piechotta, N. Neuber, B. Adam, S. Platt, L. Ruschel, N. Schnell, S.S. Riegler, H.-R. Jiang, G. Witt, R. Busch, S. Kleszczynski, Influence of powder characteristics on the structural and the mechanical properties of additively manufactured Zr-based bulk metallic glass, Mater. Des. 209 (2021) 109976.
[15] Z. Chang, W. Wang, Y. Ge, J. Zhou, Z. Cui, Microstructure and mechanical properties of Ni-Cr-Si-B-Fe composite coating fabricated through laser additive manufacturing, J. Alloys Compd. 747 (2018) 401–407, https://doi.org/10.1016/J.JALLCOM.2018.02.296.
[16] L. Deng, A. Gebert, L. Zhang, H.Y. Chen, D.D. Gu, U. Kühn, M. Zimmermann, K. Kosiba, S. Pauly, Mechanical performance and corrosion behaviour of Zr-based bulk metallic glass produced by selective laser melting, Mater. Des. 189 (2020) 108532.
[17] L. Deng, K. Kosiba, R. Limbach, L. Wondraczek, U. Kühn, S. Pauly, Plastic deformation of a Zr-based bulk metallic glass fabricated by selective laser melting, J. Mater. Sci. Technol. 60 (2021) 139–146, https://doi.org/10.1016/j.jmst.2020.06.007.
[18] X.N. Zhao, Q.P. Cao, C. Wang, X.D. Wang, D.X. Zhang, S.X. Qu, J.Z. Jiang, Dependence of room-temperature nanoindentation creep behavior and shear transformation zone on the glass transition temperature in bulk metallic glasses, J. Non. Cryst. Solids. 445–446 (2016) 19–29, https://doi.org/10.1016/j.jnoncrysol.2016.05.022.
[19] Z. Lv, C. Yuan, H. Ke, B. Shen, Defects activation in CoFe-based metallic glasses during creep deformation, J. Mater. Sci. Technol. 69 (2021) 42–47, https://doi.org/10.1016/j.jmst.2020.08.012.
[20] I.-C. Choi, B.-G. Yoo, Y.-J. Kim, M.-Y. Seok, Y. Wang, J.-i. Jang, Estimating the stress exponent of nanocrystalline nickel: Sharp vs. spherical indentation, Scr. Mater. 65 (4) (2011) 300–303, https://doi.org/10.1016/j.scriptamat.2011.04.031.
[21] M. Zhang, Y. Chen, D. Wei, L.H. Dai, Extraordinary creep relaxation time in a La-based metallic glass, J. Mater. Sci. 53 (4) (2018) 2956–2964, https://doi.org/10.1007/s10853-017-1725-y.
[22] Y. Ma, G.J. Peng, D.H. Wen, T.H. Zhang, Nanoindentation creep behavior in a CoCrFeCuNi high-entropy alloy film with two different structure states, Mater. Sci. Eng. A. 621 (2015) 111–117, https://doi.org/10.1016/j.msea.2014.10.065.
[23] F. Li, Y. Xie, J. Gu, M. Song, S. Ni, S. Guo, X. Liao, Inhomogeneous creep deformation in metallic glasses, Mater. Sci. Eng. A. 648 (2015) 57–60, https://doi.org/10.1016/j.msea.2015.09.048.
[24] B.-G. Yoo, K.-S. Kim, J.-H. Oh, U. Ramamurty, J.-i. Jang, Room temperature creep in amorphous alloys: Influence of initial strain and free volume, Scr. Mater. 63 (12) (2010) 1205–1208, https://doi.org/10.1016/j.scriptamat.2010.08.034.
[25] B.G. Yoo, J.Y. Kim, Y.J. Kim, I.C. Choi, S. Shim, T.Y. Tsui, H. Bei, U. Ramamurty, J. Il Jang, Increased time-dependent room temperature plasticity in metallic glass nanopillars and its size-dependency, Int. J. Plast. 37 (2012) 108–118, https://doi.org/10.1016/j.ijplas.2012.04.005.
[26] Y. Wang, J. Zhang, K. Wu, G. Liu, D. Kiener, J. Sun, Nanoindentation creep behavior of Cu–Zr metallic glass films, Mater. Res. Lett. 6 (1) (2018) 22–28, https://doi.org/10.1080/21663831.2017.1383946.
[27] F. Wang, J.M. Li, P. Huang, W.L. Wang, T.J. Lu, K.W. Xu, Nanoscale creep deformation in Zr-based metallic glass, Intermetallics. 38 (2013) 156–160, https://doi.org/10.1016/j.intermet.2013.03.006.
[28] P. Schall, D.A. Weitz, F. Spaepen, Structural Rearrangements That Govern Flow in Colloidal Glasses, Science (80-.) 318 (5858) (2007) 1895–1899.
[29] D. Pan, A. Inoue, T. Sakurai, M.W. Chen, Experimental characterization of shear transformation zones for plastic flow of bulk metallic glasses, Proc. Natl. Acad. Sci. USA 105 (39) (2008) 14769–14772, https://doi.org/10.1073/pnas.0806051105.
[30] Z. Wang, W.H. Wang, Flow units as dynamic defects in metallic glassy materials, Natl. Sci. Rev. 6 (2019) 304–323, https://doi.org/10.1093/nsr/nwy084.
[31] J.C. Qiao, Q. Wang, J.M. Pelletier, H. Kato, R. Casalini, D. Crespo, E. Pineda, Y. Yao, Y. Yang, Structural heterogeneities and mechanical behavior of amorphous alloys, Prog. Mater. Sci. 104 (2019) 250–329, https://doi.org/10.1016/j.pmatsci.2019.04.005.
[32] W.H. Wang, The elastic properties, elastic models and elastic perspectives of metallic glasses, Prog. Mater. Sci. 57 (3) (2012) 487–656.
[33] F. Xu, N. Zeng, K. Cheng, X. Wang, S. Long, Y. Ding, C. Yang, A study of the nanoindentation creep behavior of (La0.5Ce0.5)65Al10Co25 metallic glass

based on fractional differential rheological model, J. Non. Cryst. Solids. 490 (2018) 50–60, https://doi.org/10.1016/j.jnoncrysol.2018.03.045.
[34] W.L. Johnson, K. Samwer, A universal criterion for plastic yielding of metallic glasses with a (T/Tg)2/3 temperature dependence, Phys. Rev. Lett. 95 (2005), https://doi.org/10.1103/PhysRevLett.95.195501.
[35] W.H. Wang, Correlation between relaxations and plastic deformation, and elastic model of flow in metallic glasses and glass-forming liquids, J. Appl. Phys. 110 (2011) 053521, https://doi.org/10.1063/1.3632972.
[36] F. Dong, Y. Chu, M. He, Y. Zhang, W. Li, P.K. Liaw, B. Wang, L. Luo, Y. Su, R.O. Ritchie, X. Yuan, Manipulating Internal Flow Units Toward Favorable Plasticity in Zr-based Bulk-metallic Glasses by Hydrogenation, J. Mater. Sci. Technol. 102 (2022) 36–45, https://doi.org/10.1016/j.jmst.2021.04.037.
[37] B. Yang, L. Riester, T. Nieh, Strain hardening and recovery in a bulk metallic glass under nanoindentation, Scr. Mater. 54 (7) (2006) 1277–1280, https://doi.org/10.1016/j.scriptamat.2005.12.049.
[38] T. Burgess, M. Ferry, Nanoindentation of metallic glasses, Mater. Today. 12 (1-2) (2009) 24–32, https://doi.org/10.1016/S1369-7021(09)70039-2.
[39] W.C. Oliver, G.M. Pharr, Measurement of hardness and elastic modulus by instrumented indentation: Advances in understanding and refinements to methodology, J. Mater. Res. 19 (1) (2004) 3–20, https://doi.org/10.1557/jmr.2004.19.1.3.
[40] W.C. Oliver, G.M. Pharr, An improved technique for determining hardness and elastic modulus using load and displacement sensing indentation experiments, J. Mater. Res. 7 (6) (1992) 1564–1583.
[41] W.D. Nix, H. Gao, Indentation size effects in crystalline materials: A law for strain gradient plasticity, J. Mech. Phys. Solids. 46 (3) (1998) 411–425, https://doi.org/10.1016/S0022-5096(97)00086-0.
[42] J.-i. Jang, B.-G. Yoo, Y.-J. Kim, J.-H. Oh, I.-C. Choi, H. Bei, Indentation size effect in bulk metallic glass, Scr. Mater. 64 (8) (2011) 753–756.
[43] N. Li, K.C. Chan, L. Liu, The indentation size effect in Pd40Cu30Ni 10P20 bulk metallic glass, J. Phys. D. Appl. Phys. 41 (15) (2008) 155415, https://doi.org/10.1088/0022-3727/41/15/155415.
[44] Z.R. Xu, J.C. Qiao, J. Wang, E. Pineda, D. Crespo, Comprehensive insights into the thermal and mechanical effects of metallic glasses via creep, J. Mater. Sci. Technol. 99 (2022) 39–47, https://doi.org/10.1016/j.jmst.2021.05.036.
[45] M. Jirásek, P. Havlásek, Accurate approximations of concrete creep compliance functions based on continuous retardation spectra, Comput. Struct. 135 (2014) 155–168, https://doi.org/10.1016/j.compstruc.2014.01.024.
[46] P. Gong, J. Jin, L. Deng, S. Wang, J. Gu, K. Yao, X. Wang, Room temperature nanoindentation creep behavior of TiZrHfBeCu(Ni) high entropy bulk metallic glasses, Mater. Sci. Eng. A. 688 (2017) 174–179, https://doi.org/10.1016/j.msea.2017.01.094.
[47] C.A. Tweedie, K.J. Van Vliet, Contact creep compliance of viscoelastic materials via nanoindentation, J. Mater. Res. 21 (6) (2006) 1576–1589, https://doi.org/10.1557/jmr.2006.0197.
[48] J. Kim, G.A. Sholar, S. Kim, Determination of Accurate Creep Compliance and Relaxation Modulus at a Single Temperature for Viscoelastic Solids, J. Mater. Civ. Eng. 20 (2) (2008) 147–156, https://doi.org/10.1061/(ASCE)0899-1561(2008)20:2(147).
[49] W.H. Li, K. Shin, C.G. Lee, B.C. Wei, T.H. Zhang, Y.Z. He, The characterization of creep and time-dependent properties of bulk metallic glasses using nanoindentation, Mater. Sci. Eng. A. 478 (1-2) (2008) 371–375, https://doi.org/10.1016/j.msea.2007.06.015.
[50] X. Wang, P. Gong, L. Deng, J. Jin, S. Wang, P. Zhou, Nanoindentation study on the room temperature creep characteristics of a senary Ti16.7Zr16.7Hf16.7Cu16.7Ni16.7Be16.7 high entropy bulk metallic glass, J. Non. Cryst. Solids. 470 (2017) 27–37, https://doi.org/10.1016/j.jnoncrysol.2017.04.041.
[51] J. Kaschta, R.R. Schwarzl, Calculation of discrete retardation spectra from creep data - I. Method, Rheol. Acta. 33 (6) (1994) 517–529, https://doi.org/10.1007/BF00366336.
[52] A.H.W. Ngan, B. Tang, Viscoelastic effects during unloading in depth-sensing indentation, J. Mater. Res. 17 (10) (2002) 2604–2610, https://doi.org/10.1557/JMR.2002.0377.
[53] A. Castellero, B. Moser, D.I. Uhlenhaut, F.H.D. Torre, J.F. Löffler, Room-temperature creep and structural relaxation of Mg-Cu-Y metallic glasses, Acta Mater. 56 (15) (2008) 3777–3785, https://doi.org/10.1016/j.actamat.2008.04.021.
[54] P.F. Yu, S.D. Feng, G.S. Xu, X.L. Guo, Y.Y. Wang, W. Zhao, L. Qi, G. Li, P.K. Liaw, R. P. Liu, Room-temperature creep resistance of co-based metallic glasses, Scr. Mater. 90 (2014) 45–48, https://doi.org/10.1016/j.scriptamat.2014.07.013.
[55] F. Li, Y. Xie, M. Song, S. Ni, S. Guo, X. Liao, A detailed appraisal of the stress exponent used for characterizing creep behavior in metallic glasses, Mater. Sci. Eng. A. 654 (2016) 53–59, https://doi.org/10.1016/j.msea.2015.12.025.
[56] M.J. Mayo, W.D. Nix, A micro-indentation study of superplasticity in Pb, Sn, and Sn-38 wt% Pb, Acta Metall. 36 (8) (1988) 2183–2192, https://doi.org/10.1016/0001-6160(88)90319-7.
[57] H. Li, A.H.W. Ngan, Size effects of nanoindentation creep, J. Mater. Res. 19 (02) (2004) 513–522, https://doi.org/10.1557/jmr.2004.0063.
[58] R.S. Ginder, W.D. Nix, G.M. Pharr, A simple model for indentation creep, J. Mech. Phys. Solids. 112 (2018) 552–562, https://doi.org/10.1016/j.jmps.2018.01.001.
[59] J. Hu, W. Zhang, G. Bi, J. Lu, W. Huo, Y. Zhang, Nanoindentation creep behavior of coarse-grained and ultrafine-grained pure magnesium and AZ31 alloy, Mater. Sci. Eng. A. 698 (2017) 348–355, https://doi.org/10.1016/j.msea.2017.05.063.
[60] Z.Y. Ding, Y.X. Song, Y. Ma, X.W. Huang, T.H. Zhang, Nanoindentation investigation on the size-dependent creep behavior in a zr-cu-ag-al bulk metallic glass, Metals (Basel). 9 (2019) 613, https://doi.org/10.3390/met9050613.
[61] F. Wang, P. Huang, K.W. Xu, Time dependent plasticity at real nanoscale deformation, Appl. Phys. Lett. 90 (16) (2007) 161921, https://doi.org/10.1063/1.2730735.
[62] Z. Xu, H. Zhang, W. Li, A. Mao, L. Wang, G. Song, Y. He, Microstructure and nanoindentation creep behavior of CoCrFeMnNi high-entropy alloy fabricated by selective laser melting, Addit. Manuf. 28 (2019) 766–771, https://doi.org/10.1016/j.addma.2019.06.012.
[63] R.J. Asaro, S. Suresh, Mechanistic models for the activation volume and rate sensitivity in metals with nanocrystalline grains and nano-scale twins, Acta Mater. 53 (12) (2005) 3369–3382.
[64] L. Perrière, S. Nowak, S. Brossard, M.-T. Thai, M. Blétry, Y. Champion, Nanoindentation study of chemical effects on the activation volume controlling shear band initiation in metallic glasses, Scr. Mater. 68 (3-4) (2013) 183–186, https://doi.org/10.1016/j.scriptamat.2012.10.013.
[65] Y. Ma, G.J. Peng, T.T. Debela, T.H. Zhang, Nanoindentation study on the characteristic of shear transformation zone volume in metallic glassy films, Scr. Mater. 108 (2015) 52–55, https://doi.org/10.1016/j.scriptamat.2015.05.043.
[66] H. Idrissi, M. Ghidelli, A. Béché, S. Turner, S. Gravier, J.J. Blandin, J.P. Raskin, D. Schryvers, T. Pardoen, Atomic-scale viscoplasticity mechanisms revealed in high ductility metallic glass films, Sci. Rep. 9 (2019) 1–11, https://doi.org/10.1038/s41598-019-49910-7.
[67] M. Ghidelli, A. Orekhov, A.L. Bassi, G. Terraneo, P. Djemia, G. Abadias, M. Nord, A. Béché, N. Gauquelin, J. Verbeeck, J.-P. Raskin, D. Schryvers, T. Pardoen, H. Idrissi, Novel class of nanostructured metallic glass films with superior and tunable mechanical properties, Acta Mater. 213 (2021) 116955, https://doi.org/10.1016/j.actamat.2021.116955.
[68] N. Adachi, Y. Todaka, Y. Yokoyama, M. Umemoto, Improving the mechanical properties of Zr-based bulk metallic glass by controlling the activation energy for β -relaxation through plastic deformation, Appl. Phys. Lett. 105 (13) (2014) 131910, https://doi.org/10.1063/1.4897439.
[69] Y. Ma, G.J. Peng, Y.H. Feng, T.H. Zhang, Nanoindentation investigation on the creep mechanism in metallic glassy films, Mater. Sci. Eng. A. 651 (2016) 548–555, https://doi.org/10.1016/j.msea.2015.11.014.
[70] C. Wang, Q.P. Cao, X.D. Wang, D.X. Zhang, S.X. Qu, J.Z. Jiang, Time-dependent shear transformation zone in thin film metallic glasses revealed by nanoindentation creep, J. Alloys Compd. 696 (2017) 239–245, https://doi.org/10.1016/j.jallcom.2016.11.264.
[71] C. Zhang, D. Zhou, B. Hou, Influence of Defects to Zr65Cu18Ni7Al10 Bulk Metallic Glass Properties Under Dynamic Compression, Front. Mater. 8 (2022) 1–8, https://doi.org/10.3389/fmats.2021.820158.
[72] F. Dong, M. He, Y. Zhang, B. Wang, L. Luo, Y. Su, H. Yang, X. Yuan, Investigation of shear transformation zone and ductility of Zr-based bulk metallic glass after plasma-assisted hydrogenation, Mater. Sci. Eng. A. 759 (2019) 105–111, https://doi.org/10.1016/j.msea.2019.05.027.